Snow processes in mountain forests: Interception modeling for coarse-scale applications

Nora Helbig[1], David Moeser[2], Michaela Teich[3,4], Laure Vincent[5], Yves Lejeune[5], Jean-Emmanuel Sicart[6], and Jean-Matthieu Monnet[7]

[1]WSL Institute for Snow and Avalanche Research SLF, Davos, Switzerland
[2]USGS, New Mexico Water Science Center, Albuquerque, USA
[3]Austrian Research Centre for Forests (BFW), Innsbruck, Austria
[4]Department of Wildland Resources, Utah State University, Logan, UT, USA
[5]University Grenoble Alpes, University Toulouse, Météo-France, CNRS, CNRM, Centre d'Etudes de la Neige, Grenoble, France
[6]Université Grenoble Alpes, CNRS, IRD, Grenoble INP, Institut des Géosciences de l'Environnement (IGE) - UMR 5001, F-38000 Grenoble, France
[7]Univ. Grenoble Alpes, Irstea, LESSEM, 38000 Grenoble, France

Correspondence: Nora Helbig, (norahelbig@gmail.com)

Abstract. Snow interception by forest canopy drives the spatial heterogeneity of subcanopy snow accumulation leading to significant differences between forested and non-forested areas at a variety of scales. Snow intercepted by forest canopy can also drastically change the surface albedo. As such, accurately modelling snow interception is of importance for various model applications such as hydrological, weather and climate predictions. Due to difficulties in direct measurements of snow inter-

5   ception, previous empirical snow interception models were developed at just the point scale. The lack of spatially extensive data sets has hindered validation of snow interception models in different snow climates, forest types and at various spatial scales and has reduced accurate representation of snow interception in coarse-scale models. We present two novel models for the spatial mean and one for the standard deviation of snow interception derived from an extensive snow interception data set collected in a spruce forest in the Swiss Alps. Besides open area snowfall, subgrid model input parameters include the standard

10   deviation of the DSM (digital surface models) and the sky view factor, both of which can be easily pre-computed. Validation of both models was performed with snow interception data sets acquired in geographically different locations under disparate weather conditions. Snow interception data sets from the Rocky Mountains, U.S. and the French Alps compared well to modelled snow interception with a NRMSE for the spatial mean of ≤ 10 % for both models and NRMSE of the standard deviation of ≤ 13 %. Our results suggest that the proposed snow interception models can be applied in coarse land surface model grid

15   cells provided that a sufficiently fine-scale DSM of the forest is available to derive subgrid forest parameters.

1   Introduction

Snow interception is the amount of snow captured in the forest canopy. In winter as much as 60 % of the cumulative snowfall may be retained in conifer forests (Pomeroy and Schmidt, 1993; Pomeroy et al., 1998; Storck and Lettenmaier, 2002) and as

much as 24 % of total annual snowfall may be retained in deciduous forests in the Southern Andes (Huerta et al., 2019). Due

20   to the sublimation of intercepted snow, a large portion of this snow never reaches the ground (Essery et al., 2003) and the interplay of interception and sublimation creates significant below forest heterogeneity in snow accumulation. Rutter et al. (2009) estimated that 20 % of the seasonal snow cover within the Northern Hemisphere is located within forested areas. As such, the mass balance of solid precipitation in forested regions, characterized by strong spatial variability of snow accumulation, is a large contributor to the global water budget. Accurately modeling the spatial distribution of snow water equivalent in forested

25   regions is thus necessary for climate and water resource modeling over a variety of scales (see Essery et al., 2009; Rutter et al., 2009). Surface albedo is a significant driver of the global surface energy balance and precise albedo estimations are critical for a range of model applications such as climate scenarios (Hall, 2004). However, intercepted snow can drastically change surface albedo values in forested regions. Previous studies observed large albedo differences (a range of 30 %) between snow-free and snow-covered forest stands (e.g. Roesch et al., 2001; Bartlett and Verseghy, 2015; Webster and Jonas, 2018). Thus, in

30   mountainous areas where forested and alpine regions coexist, accurate estimates of forest albedo play a key role in correctly modeling the surface energy balance. Due to the connectivity between interception and albedo, formulations of surface albedo over forested areas necessitate estimates of intercepted snow (e.g. Roesch et al., 2001; Roesch and Roeckner, 2006; Essery, 2013; Bartlett and Verseghy, 2015).

So far, direct snow interception measurements have only been retrieved from weighing trees. These measurements are limited

35   to the point scale, are resource intensive sampling and only allow for analysis of small to medium size trees, or tree elements (Schmidt and Gluns, 1991; Hedstrom and Pomeroy, 1998; Bründl et al., 1999; Storck and Lettenmaier, 2002; Knowles et al., 2006; Suzuki and Nakai, 2008). However, there are indirect techniques which allow for estimations of interception over larger spatial scales. Indirect measurements that compare snow accumulation between open and forest sites allow for a larger spatial sampling but can be affected by other snow forest processes, such as by snow unloading. As such, sample timing of snow storm

40   conditions needs to be evaluated (e.g. Satterlund and Haupt, 1967; Schmidt and Gluns, 1991; Hedstrom and Pomeroy, 1998; Moeser et al., 2015b). Until recently, snow interception could not be characterized over spatial scales on the order of several tens of meters at which scale snow interception can spatially vary due to canopy heterogeneity.

Several statistical parameterizations for forest interception snow depth (I_{HS}) and snow water equivalent (I_{SWE}) have been suggested using a variety of canopy metrics and functional dependencies for the rate and amount of storm snowfall (e.g.

45   Satterlund and Haupt, 1967; Schmidt and Gluns, 1991; Hedstrom and Pomeroy, 1998; Hellström, 2000; Lundberg et al., 2004; Andreadis et al., 2009; Moeser et al., 2015b; Huerta et al., 2019; Roth and Nolin, 2019). Though these parameterizations have been demonstrated to perform well, they often rely on detailed forest canopy density and structure metrics which are either not readily available or cannot easily be upscaled, limiting functionality in models where the mean of model grid cells over several hundreds of meters to a few kilometers is required, i.e. potentially reducing validity in large scale modeling efforts.

50   Traditional forest metrics used to parameterize snow interception include leaf area index (LAI), canopy closure (CC) and canopy gap fraction (GF) or sky view. These are mainly derived from hemispheric photographs (HP) taken from the forest floor looking upwards. However, these indices can also be estimated from synthetic hemispheric photographs (SP). SP images mimic HP images but are generated from aerial LiDAR (light detection and ranging) data. This requires the inversion

of LiDAR to a ground perspective and conversion from a Cartesian to a polar coordinate system (Moeser et al., 2014). Prior

55 work has also used return density ratios of LiDAR, which is computationally faster but less accurate than SP images (Morsdorf et al., 2006). Canopy structure, or the position of a canopy element relative to the surrounding forest canopy, have also been used to model snow interception. However, as pointed out by Moeser et al. (2015b), some forest structure metrics such as LAI and CC are highly cross-correlated. Moeser et al. (2015b, 2016) expanded on prior interception models, which mostly rely on the highly cross-correlated traditional forest density parameters LAI and CC by introducing uncorrelated novel forest

60 structure metrics. Their empirical interception model utilizes total open area, mean distance to canopy and CC. While the latter parameter was derived from SP (Moeser et al., 2014), the first two parameters were directly computed from a DSM. Total open area is defined as the total open area in the canopy around a point and mean distance to canopy defines how far away the edge of the canopy is from a point. Recently Roth and Nolin (2019) extended mean distance to canopy vertically, by deriving it for 1 m horizontal slices that were normalized with the corresponding elevation above the ground.

65 Due to the difficulties in measuring snow interception, previous empirical snow interception models were not validated in different snow climates, forest types or at varying spatial scales. During SNOWMIP2 (Essery et al., 2009; Rutter et al., 2009), where 33 snow models were validated at individual forested as well as open sites, many models used the snow interception parameterization from Hedstrom and Pomeroy (1998). This interception model was one of the first that used canopy metrics (LAI and CC). Though, a snow interception model for larger scales also requires the greater canopy structure. Overall,

70 SNOWMIP2 showed that maximum snow accumulation predictions had large errors compared to observed values in most models but snow cover duration was well estimated. Furthermore, a universal best model could not be found since model performances at forest sites varied. This may explain why there is still no common ground with several snow-related variables in land surface models (Dirmeyer et al., 2006) which led to the current Earth System Model-Snow Model Intercomparison Project (ESM-SNOWMIP) showing overall larger errors in simulated snow depth on forest sites than on open sites (Krinner et al.,

75 2018). Recently Huerta et al. (2019) validated three previous snow interception models developed for coniferous forests with observed point snow interception values in a deciduous *Nothofagus* -forest of the Southern Andes. All three empirical models required recalibration, with the recalibrated Hedstrom and Pomeroy (1998) model showing the overall best performance. Similarly, model simulations of Vincent et al. (2018) largely overestimated observed accumulated snow depth in a spruce forest at Col de Porte in the Southeastern French Alps. They attribute this to errors in the processes linked to the snow interception

80 model based on Hedstrom and Pomeroy (1998) due to an underestimation of the melt of intercepted snow. Previous snow interception models also failed to accurately model snow interception from a maritime climate (Roth and Nolin, 2019). While Roth and Nolin (2019) successfully modelled snow interception by including air temperature in a maritime climate, their model consistently underestimates snow interception in a continental climate forest. Overall, this demonstrates the need for more robust parameterizations of the processes affecting snow under forest which is an important challenge for global snow

85 modeling.

When modeling at resolutions greater than the point scale, accurate implementation of forest snow processes necessitates not just the mean of a grid cell but the standard deviation within a grid cell or model domain. However, to our knowledge, the standard deviation of snow interception has not yet been quantified. In this paper, we propose empirical parameterizations for

the spatial mean and standard deviation of snow interception depth derived from indirect interception measurements at sites

90 with length scales on the order of several tens of meters. We analyzed an extensive data set consisting of several thousand interception measurements collected immediately after storm events in a discontinuous coniferous forest stand in the Eastern Swiss Alps (Moeser et al., 2014, 2015a, b, 2016). From a LiDAR digital surface model (DSM) with elevations z (Moeser et al., 2014), we derived two canopy structure metrics: (1) the standard deviation of the DSM (σ_z) in order to represent the spatial heterogeneity of canopy height in a model domain and (2) spatial mean sky view factor (F_{sky}) which roughly represents the

95 spatial mean canopy openness but is derived here on the Cartesian DSM from geometric quantities that describe the received radiative flux fraction emitted by another visible surface patch (i.e. canopy patches) (Helbig et al., 2009). These two metrics were correlated to spatial means of the indirect interception measurements. We validated the novel parameterizations with new indirect snow interception measurements from one site located in the Rocky Mountains of Northern Utah, United States and from one site located at Col de Porte in the Southeastern French Alps.

100 ## 2 Data

2.1 Eastern Swiss Alps

Indirect interception measurements were collected in seven discontinuous coniferous forest stands near Davos, Switzerland at elevations between 1511 m and 1900 m consisting of primarily Norway spruce (*Picea abies*) (Fig. 1a). Mean annual air temperature in Davos (1594 m) is approximately 3.5 °C and the average solid precipitation is 469 cm per year (climate normal

105 1981-2010, MeteoSwiss). The field sites are maintained and operated by the Snow Hydrology group of the WSL Institute for Snow and Avalanche research SLF in Davos, Switzerland. The sites were chosen to limit influence of slope and topographic shading while capturing as much diversity as possible in elevation, canopy density and canopy structure (Fig. 2). Each of the seven field areas were equipped in the same manner and consisted of 276 marked and georectified measurement points (about ±50 cm) over a 250 m^2 surface area (Fig. 1a). Two non-forested (open field area) reference sites were also equipped to derive

110 the indirect snow interception measurements.

During the winters of 2012/2013 and 2013/2014, snow depth was measured at all field points, immediately after every storm with greater than 15 cm depth of open area snowfall. In total, nine storm events met the following pre-storm and storm conditions that allowed for indirect interception measurements: (1) no snow in canopy prior to a storm event, (2) defined crust on the underlying snow, and (3) minimal wind redistribution during the storm cycle. New snow was measured down to the prior

115 snow layer crust to the top of the newly fallen snow layer to represent total snow interception. Total snow fall was measured at the open field areas. The extensive measurement data set used in this study was previously published in high detail in Moeser et al. (2014, 2015a, b, 2016). For this study, 13994 of the individual measurements were used to compute 60 site based mean and standard deviation values of snow interception, which were then utilized to develop the interception parameterizations. For all individual measurements, a mean snow interception efficiency (interception / new snowfall open) of 42 % was measured

120 with values ranging from 0 to 100 %. The probability distribution function (*pdf*) of all snow interception data can be fitted with a normal distribution with a Root-Mean-Square Error (RMSE) of the quantiles between both distributions of 0.6 cm and

a Pearson correlation r of 0.99 for the quantiles (Fig. 3). Average storm values of air temperatures covered cold (-12.1 °C) to mild (-1.9 °C) conditions.

125   A 1 m^2 resolution LiDAR DSM was generated from a flyover in the summer of 2010 and encompasses all Eastern Swiss Alps field areas (Fig. 1a). The initial point cloud had an average density of 36 points/m^2 and a shot density of 19 points/m^2 (last return). The 1 m^2 resolution LiDAR DSM is used for the derivation of the canopy structure metrics, the standard deviation of the DSM (σ_z) and the spatial mean sky view factor (F_{sky}) over each 50x50m^2 field site.

2.2   Rocky Mountains of Northern Utah in the United States

For the first validation data set, indirect interception measurements were collected at Utah State University's T.W. Daniel
130 Experimental Forest (TWDEF; 41.86°N, 111.50°W) that is located at ∼2700 m a.s.l. in the Rocky Mountains of Northern Utah (Fig. 1b). The forest stand is predominantly coniferous and is composed of Engelman spruce (*Picea engelmannii*) and subalpine fir (*Abies lasiocarpa*). However, there are deciduous aspen (*Populus tremuloides*) forest stands present. Mean annual air temperature is approximately 4°C and mean annual precipitation is approximately 1080 mm (PRISM Climate Group, 2012). On average 80 % of the precipitation falls as snow. Similar to the sites in the Eastern Swiss Alps, two forested sites and one
135 non-forested site were chosen to limit influence of slope and topographic shading while capturing diversity in canopy density and canopy structure.

    At one forested site, total snow depth measurements were taken before and after two storm events during winter 2015/2016 along four parallel 20-m forested transects every 0.5 m (Fig. 1b) as well as at a non-forested meadow location (open site). At the second forested site, only one snow storm was captured by pre- and post-storm total snow depth measurements along two
140 parallel 20-m transects. Since the purpose of the Utah measurement campaigns was not to measure snow interception but rather to investigate spatial variability of snow characteristics below different forest canopies (Teich et al., 2019), the derivation of snow interception differed from the Swiss sites. Interception was estimated as the difference between pre- and post-storm snow depth. Post-storm measurements were taken anywhere between approximately one to three days after a recent snowfall. The storm events were also temporally close, so that all the trees were not snow free prior to new snowfall. As such, unloading and
145 snow settling may have influenced these measurements. After parsing the data to further reduce such influences, 95 individual interception measurements remained, resulting in three site means and three standard deviations to validate parameterizations developed from the Swiss data set. For all individual measurements, a mean snow interception efficiency of 33 % was measured with values ranging from 2 to 93 %. The *pdf* of all individual snow interception data can be similarly well fitted with a normal distribution with a RMSE of the quantiles between both distributions of 1.3 cm and a Pearson correlation r of 0.98 for the
150 quantiles (Fig. 3). Average storm values of air temperatures covered cold (-7.33 °C) to mild (-1.4 °C) conditions.

    A 1 m^2 resolution LiDAR DSM was generated from a flyover in July of 2009 and encompasses all field areas (Mahat and Tarboton, 2012; Teich and Tarboton, 2016) (Fig. 1b). The initial point cloud had on average 7 returns/m^2 and 5 last returns/m^2 (shot density). The 1 m^2 resolution LiDAR DSM is used for the derivation of the canopy structure metrics σ_z and F_{sky} over each 20-m transect (field site).

2.3 Southeastern French Alps

For the second validation data set, indirect interception measurements were collected in a coniferous forest stand next to the mid-altitude experimental site Col de Porte (45.30°N, 5.77°E) at 1325 m a.s.l. in the Chartreuse mountain range in the French Alps (more site details in Morin et al. (2012); Lejeune et al. (2019)). The dominant forest stand is Norway spruce (*Picea abies*), with young silver fir (*Abies alba*) in the understory. Small deciduous trees are present along the north-west border of the experimental site. Mean annual air temperature is 6°C and the average solid precipitation at Col de Porte is 644 mm per year.

New snow depth measurements were collected in one forested field area during pre- and post-storm events by the Snow Research Center (Centre d'Etude de la Neige (CEN))) in Grenoble, France as part of the Labex SNOUF project (SNow Under Forest) (Fig. 1c) next to the Col de Porte experimental site (Vincent et al., 2018). There were three 8-m transects, each consisting of eight 1 m x 0.39 m wooden boxes that were aligned along the North, South and West axes of the field area. New snow depth was measured inside each box after a storm event and was then cleared of snow. Open area new snow depth measurements were obtained from snow board measurements from the Col de Porte experimental site. The boards were cleaned after each precipitation event. Interception was then derived as the difference between the open area and under-canopy snow box measurements. Snow depth was collected after a major storm event took place. Unloading was visually observed from webcams. As such, unloading had a minimal influence on the measurements. Four snow storm events during 2018 were selected for a total of 96 individual interception measurements (4x24 measurements) and resulted in four site means and standard deviation values for the second independent validation data set. For the individual measurements, a mean snow interception efficiency of 66 % was measured with values ranging from 1 to 94 %. The *pdf* of all snow interception data can be roughly fitted with a normal distribution with a RMSE of the quantiles between both distributions of 1.1 cm and a Pearson correlation r of 0.96 for the quantiles (Fig. 3). Average storm values of air temperatures covered mild (-0.9 °C) to warm (1.7 °C) conditions.

A 1 m^2 resolution LiDAR DSM was generated from a flyover between 30 August and 2 September 2016 and encompasses the entire Col de Porte experimental site (IRSTEA, Grenoble (Fig. 1c)). The initial LiDAR point cloud had an average density of 24 points /m^2 and a shot density of 17 points/ m^2 (last return). The initial point cloud right at the transects had an average density of 42 points /m^2 and a shot density of 25 points/ m^2 (last return). The 1 m^2 resolution LiDAR DSM is used for the derivation of the canopy structure metrics σ_z and F_{sky} over the three 8-m transects.

3 Methods

Subgrid parameterizations were derived for site means and standard deviation of snow interception using forest structure metrics and open area snowfall. We parameterize mean and spatial variability of snow interception for a model grid cell by accounting for the unresolved underlying forest structure (subgrid parameterization).

3.1 Forest structure metrics

The sky view factor F_{sky} describes the proportion of a radiative flux received by an inclined surface patch from the visible part of the sky to that obtained from an unobstructed hemisphere (Helbig et al., 2009). F_{sky} is a commonly applied model parameter when computing surface radiation balances and can be easily computed for large areas from DSM's. F_{sky} integrates previously applied forest structure metrics, such as total open area and mean distance to canopy, since this parameter is able to account for distance, size and orientation of individual surface (or canopy) patches (Helbig et al., 2009). We therefore selected F_{sky} to parameterize the site mean and standard deviation of snow interception (I_{HS}, σ_{HS}). Here, we compute F_{sky} from view factors which are geometrically derived quantities. They can be computed by numerical methods described within the radiosity approach for the shortwave (SW) radiation balance over complex topography (Helbig et al., 2009) and were originally introduced to describe the radiant energy exchange between surfaces in thermal engineering (Siegel and Howell, 1978). Thereby, Helbig et al. (2009) solve the double area integral using uniform but adaptive area subdivision for surface patches A_I, A_J. F_{sky} for each surface patch A_I is one minus the sum over all N view factors F_{IJ} by assuming the sky as one large surface patch:

$$F_{I,sky} = 1 - \sum_{J=1}^{N} F_{IJ} = 1 - \sum_{J=1}^{N} \frac{1}{A_I} \int\limits_{A_I} \int\limits_{A_J} \frac{\cos\vartheta_I \ \cos\vartheta_J}{\pi \ r_{IJ}^2} \, \mathrm{d}A_I \, \mathrm{d}A_J \ . \tag{1}$$

Deriving F_{sky} via Eq. (1) can account for holes in the surface, i.e. small gaps between leaves and branches in forest canopy, provided the DSM is of a high enough resolution to capture this. In this study, the employed DSM's did not resolve small gaps between branches. Common methods to derive F_{sky} for forested regions is from sine and cosine weighted proportions of sky pixels of HP or SP as suggested e.g. by Essery et al. (2008) or from LAI (e.g. Roesch et al., 2001). However, compared to computing F_{sky} on DSM's these methods rely on extensive field work. The main advantage in deriving F_{sky} on DSM's is that F_{sky} can be derived spatially. Here, we use the spatial mean of the sky view factor F_{sky} over a field site which is comparable to the spatial mean canopy openness.

The second forest structure metric selected was the standard deviation of the DSM σ_z of a field area. Though not totally uncorrelated from the spatial mean F_{sky} (Pearson r=-0.41), we selected σ_z to serve in coarse-scale models that are not able to rely on computational expensive pre-computations of F_{sky} on fine scales, such as land surface models covering regions of several hundreds to thousands of kilometers. σ_z is thought to represent the spatial heterogeneity of canopy height of the field site (or model domain).

3.2 Subgrid parameterization for forest canopy interception

Parameterizations for site mean and standard deviation of snow interception were derived from the 60 measured mean and standard deviation values from the Swiss data set. Estimates derived using the new parameterizations were validated from a comparison to the mean and standard deviation values from the French and U.S. field sites. However, snow interception I was modeled as snow depth HS, i.e. I_{HS}, and not as snow water equivalent SWE to remove any potential error when converting measured HS values to SWE. Previous interception models (Hedstrom and Pomeroy, 1998; Schmidt and Gluns,

1991; Moeser et al., 2015b) estimated new snow density to convert HS into SWE. Models of new snow density typically rely on average storm temperature. This introduces a bias and prior work has shown a standard error of 9.31 kg/m^{-3} when using estimates of density (Hedstrom and Pomeroy, 1998). As such, the snow interception parameterizations developed here are for
220   HS.

From here on, all references will be to site values (mean and standard deviation) without explicitly mentioning the 'mean', unless otherwise stated.

3.3   Performance measures

We use a variety of measures to validate the parameterizations: the Root-Mean-Square Error (RMSE), Normalized Root-Mean-
225   Square Error (NRMSE) (normalized by the range of data), Mean-Absolute Error (MAE), the Mean Percentage Error (MPE) (Bias with measured-parameterized normalized with measurements) and the Pearson correlation coefficient r as a measure for correlation. Finally, we evaluate the performance of our parameterizations by analyzing the pdf's. We use the two-sample Kolmogorov-Smirnov test (K-S test) statistic values D for the pdf's (nonparametric method) and compute the NRMSE for Quantile-Quantile plots (NRMSE$_{\text{quant}}$) for probabilities with values in $[0.1, 0.9]$.

230   ## 4   Results

4.1   Grid cell mean snow interception

4.1.1   Parameterization

We parameterized grid cell mean intercepted snow depth (I_{HS}) by scaling open area accumulated snowfall P_{HS} using the forest structure metrics F_{sky} and σ_z. From these three variables, the interception measurements of the development data set
235   correlated best with P_{HS} ($r = 0.70$). Snow interception efficiency (I_{HS}/P_{HS}) correlations were slightly stronger for σ_z ($r = 0.71$) than for F_{sky} ($r = -0.63$).

Based on observed relationships and correlations we developed two statistical parameterizations for I_{HS} using two different base functions to scale P_{HS} with either F_{sky} and σ_z (Eq. (2)) or with only σ_z (Eq. (3)):

$$I_{HS} = P_{HS}^{\text{a}} \frac{(1 - F_{\text{sky}}^{\text{b}})\,\sigma_z^{\text{c}}}{1 + exp(-\text{d}(P_{HS} - \text{f}))} \tag{2}$$

with constant parameters: a$= 0.6417$, b$= 1.0868$, c$= 0.7063$, d$= 0.1597$ and f$= 6.6884$ and

$$I_{HS} = P_{HS}^{\text{a}^{\star}}\,\text{b}^{\star}\,\sigma_z^{\text{c}^{\star}} \tag{3}$$

240   with constant parameters: a$^{\star} = 0.8199$, b$^{\star} = 0.1424$ and c$^{\star} = 0.8002$. The constant parameters resulted from fitting non-linear regression models by robust M-estimators using iterated reweighed least squares (see R v3.2.3 statistical programming language robustbase v0.92-5 package (Rousseeuw et al., 2015)).

The accuracy of a derived model between I_{HS} and P_{HS} depended upon the forest structure metrics and the underlying function applied in the potential models. The best performances were seen when the base function between I_{HS} and P_{HS} was

245   either a power law or a combination of a power law with an exponential dependence similar to the one suggested by Moeser et al. (2015b).

Estimated I_{HS}-values from Eq. (2) or (3) increase with increasing P_{HS}, increasing σ_z or decreasing F_{sky}. This implies that with decreasing forest density (i.e. more canopy surface is exposed), I_{HS} increases faster with increasing P_{HS}. Note that here, a lower F_{sky} value denotes more pronounced forest gaps since it is derived from aerial LiDAR DSM in contrast to ground based

250   HP acquired below canopy, where this relationship is reversed.

Eq. (2) and (3) differ in two ways. First, Eq. (2) incorporates the functional dependency for increasing P_{HS} that snow interception efficiency (interception/snowfall) increases with increasing precipitation due to snow bridging between branches until a maximum is reached after which it decreases due to bending of branches under the load (sigmoid curve as suggested by Moeser et al. (2015b)). Additionally, a power law dependency for accumulated open area storm snowfall is applied to force

255   the sigmoid distribution to zero at very small snowfall events. The sigmoid curve alone is not able to reach zero, potentially breaking the mass balance. In contrast, Eq. (3) solely employs the power law dependency between I_{HS} and accumulated open area storm snowfall P_{HS}. The second difference between both equations is that Eq. (2) uses both forest structure metrics (F_{sky} and σ_z), whereas Eq. (3) only uses σ_z. Eq. (2) is thus more 'complex,' and necessitates more time to derive both forest structure parameters whereas Eq. (3) has a more 'compact' form and solely necessitates estimation of σ_z.

260   **4.1.2   Validation**

Performances of both newly developed snow interception I_{HS} models (Eq. (2) and (3)) were compared to the I_{HS} measurements from the development data set (Switzerland), as well as the I_{HS} measurements from the combined two geographically and climatological different validation data sets (France and United States). In Figs. 4 to 6 we differentiate the validation data set from the development data set by using a black outline around the symbols (validation) instead of colored circles

265   (development). Squares represent the data set from the U.S. and diamonds represent the data set from France.

Fig. 4 displays that, for both models, there is a good agreement for I_{HS} to measured interception at all sites. Overall error statistics show good performances for the development and the validation data sets with low absolute errors (e.g. all MAE$\leq$1.2 cm), strong correlations (all $r \geq$0.9) and low distribution errors (e.g. all NRMSE$_{quant}$ lower 10 %) (Table 1). In contrast to the validation data sets performance statistics for the development data set are slightly reduced for the more compact model (Eq.

270   (3)) compared to the more complex model (Eq. (2)).

Fig. 5 reveals overall similar performances for both parameterizations as a function of accumulated snow fall. However, small differences between both parameterizations are visible in the extremes, i.e. for very low and very large I_{HS} and P_{HS}. The bias for the largest P_{HS} (U.S. data set) is slightly larger for the more complex parameterization (Eq. (2)) whereas for the smallest P_{HS} (data set from France) the bias is larger for the more compact parameterization (Eq. (3)). The bias is more

275   pronounced with regard to the corresponding interception efficiencies, shown in Fig. 5d-f, the largest bias for the smallest P_{HS} for the compact parameterization (Eq. (3)) is -0.23 compared to 0.09 for the more complex parameterization (Eq. (2)).

4.2 Grid cell standard deviation of snow interception

4.2.1 Parameterization

We parameterized the standard deviation of snow depth interception $\sigma_{I_{HS}}$ by scaling P_{HS} using the forest structure metric σ_z.
280   $\sigma_{I_{HS}}$ of the development data set correlated best with P_{HS} ($r = 0.82$). The correlation with I_{HS} was less pronounced ($r =$ 0.33). $\sigma_{I_{HS}}$ normalized with P_{HS} correlated much better with σ_z ($r = -0.68$) than with F_{sky} ($r = 0.1$).

Building upon the observed power law functional dependency between mean snow interception I_{HS} and P_{HS} and the observed relationships and correlations for $\sigma_{I_{HS}}$ we scaled a power law function for P_{HS} with the standard deviation of the DSM σ_z in order to parameterize $\sigma_{I_{HS}}$:

$$\sigma_{I_{HS}} = P_{HS}^{g}\, h\, \sigma_z^{j} . \tag{4}$$

285   Constant parameters g$= 0.7821$, h$= 1.0826$ and j$= -0.5175$ result from fitting a non-linear regression model, similar to the derivation of I_{HS} from Eq. (2) and (3). $\sigma_{I_{HS}}$ derived from Eq. (4) increases with increasing P_{HS} or decreasing σ_z. This implies that as canopy height becomes more homogeneous, the spatial variability in snow interception increases faster with increasing P_{HS}.

4.2.2 Validation

290   Overall, modeled and measured $\sigma_{I_{HS}}$ agree well (Fig. 6). Error statistics show good performances for the development and the validation data set with low absolute errors (e.g. all MAE$\leq$0.64 cm), strong correlations (all $r \geq$0.92) and low distribution errors (e.g. NRMSE$_{quant}$ lower 10 %) (Table 1). However, performances are less accurate for the validation data set than for the development data set (e.g. MAE of 0.64 cm as opposed to 0.45 cm and NRMSE$_{quant}$ of 10 % as opposed to 4 %). This was caused by a potential outlier in the validation data set from the U.S. During one measurement campaign, an open area
295   accumulated storm snowfall P_{HS} was not available at the same date as the under canopy measurements. Therefore, this value was estimated from a local automatic weather station (Usu Doc Daniel SNOTEL site). Additional measurement uncertainty (at the Utah site) was also introduced, since interception estimates were integrated values over several snow storms that occurred during the 13 days between pre- and post- snowfall measurement campaigns. When this outlier is removed from the validation data set, performance statistics improve considerably converging towards the errors of the development data set, cf. MAE
300   decreases to 0.35 cm and the NRMSE$_{quant}$ to 5 %.

To compare modeled and measured data set mean values from each geographic location (Switzerland, US, France), we averaged all site values to derive overall mean of I_{HS}, and $\sigma_{I_{HS}}$ for each location. The coefficient of variation (description of variability) ($CV_{I_{HS}}=\sigma_{I_{HS}}/I_{HS}$) was also calculated for each of the three geographic locations. For the Swiss development data set, the same overall mean and standard deviation for measured and modeled snow interception was calculated (mean of
305   4.5 cm and standard deviation of 9.4 cm), and the CV was almost equivalent (0.51 versus 0.50). For the validation data sets we obtained slightly larger values for modeled I_{HS} (9.4 cm), modeled $\sigma_{I_{HS}}$ (3.7 cm) and modeled $CV_{I_{HS}}$ (0.40) than measured I_{HS} (9.2 cm), measured $\sigma_{I_{HS}}$ (3.2 cm) and measured $CV_{I_{HS}}$ (0.35). If the potential outlying data point from Utah is removed,

the same overall modeled and measured mean $CV_{I_{HS}}$ (0.31) is found along with very close values of modeled and measured mean I_{HS} (10.1 cm versus 9.9 cm) and modeled and measured $\sigma_{I_{HS}}$ values (3.4 cm versus 3.3 cm).

310 5 Discussion

We proposed two models for spatial mean interception I_{HS} to be employed in hydrological, climate and weather applications. One model is a more compact model, Eq. (3). This model uses a power law dependency between I_{HS} and accumulated storm precipitation P_{HS} that is scaled by one forest structure metric: the standard deviation of the DSM σ_z. The other model, Eq. (2), integrates a more complex parameterization by using a combination of a power law with an exponential dependence similar to

315 the one suggested by Moeser et al. (2015b) for P_{HS} and is scaled by two forest metrics: the sky view factor F_{sky} in combination with σ_z. For both I_{HS} models, interception increases faster with increasing snowfall when forest density decreases (i.e. more canopy is exposed). In the more complex model decreasing forest density is implemented by increasing σ_z and decreasing F_{sky}. Though F_{sky} can be pre-computed and is temporally valid for many years (unless the forest structure changes due to logging, fires, insect infestations or other forest disturbances), computing F_{sky} over large scales and/or with fine resolutions

320 is more computationally demanding than for σ_z (Helbig et al., 2009). A subgrid parameterization for the sky view factor of coarse-scale DSM's over forest canopy would eliminate the pre-computation of sky view factors on fine-scale DSM's. Such a subgrid parameterization for sky view factors over forest canopy could be similarly set up as previously done for alpine topography and lead us towards a global map of sky view factors (cf. Helbig and Löwe, 2014).

In general, more differences between the compact and more complex modeling approaches only displayed at the extremes.

325 For instance, for small storm precipitation values (P_{HS} =3 cm), the more complex parameterization performs better whereas for very large storms (P_{HS} =43 cm), the more compact model displayed improved performance. The choice for one of these two models thus depends on field area characteristics, desired accuracy and available computational resources.

We have derived just one model for the standard deviation of snow interception $\sigma_{I_{HS}}$ that uses a power law dependency on accumulated storm precipitation P_{HS} scaled by one forest structure metric: the standard deviation of the DSM σ_z. We also

330 tested a more complex model for $\sigma_{I_{HS}}$ using both forest metrics (F_{sky} and σ_z) that also integrates a power law dependency of P_{HS}. However, model performances for the validation data set did not differ considerably from the ones for the more compact model. Therefore, we propose the more compact parameterization for $\sigma_{I_{HS}}$ (Eq. (4)) to facilitate broad model applications.

By using F_{sky} and σ_z derived from DSM's as forest structure metrics we focused on the overall shape of the forest. This simplification is similar to the assumption by Sicart et al. (2004) for solar transmissivity in forests under cloudless sky condi-

335 tions. They assumed the fraction of solar radiation blocked by the canopy was equal to 1-Vf_f with V_f therein being defined as the fraction of the sky visible from beneath the canopy. Our simplification is also in line with previous suggestions. Primarily, to reliably describe interception by forest canopy over larger areas, the larger-scale canopy structure needs to be taken into account instead of only using point based canopy structure parameters (e.g. Varhola et al., 2010; Moeser et al., 2016).

The models for I_{HS} and $\sigma_{I_{HS}}$ were statistically derived from measured snow interception data gathered in the Eastern

340 Swiss Alps. We displayed that the parameterizations perform well for two disparate snow interception data sets collected in

geographically different regions, different snow climates, tree species and prevailing weather conditions during collection of the validation data sets (French Alps and Rocky Mountains). For instance, in the French Alps, rather warm to mild winter weather conditions predominated whereas rather mild to cold weather prevailed during the campaigns in the Rocky Mountains of Northern Utah in the U.S. Though snow cohesion and adhesion are clearly temperature dependent, we did not observe

345   decreases in overall performances under these differing weather conditions for our two I_{HS} models, which do not include air temperature. In contrast, in a maritime (warm) snow climate correlations between air temperature and snow interception were recently found Roth and Nolin (2019). Our ranges of interception and accumulated snow storm P_{HS} values of the development data set are fairly broad (e.g. P_{HS} between 10 cm and 40 cm). The measurements of the validation data set are well within the range of the development data set values, with the exception of one very small (P_{HS}= 3 cm) and one very

350   large snow fall (P_{HS}= 43 cm) (cf. Fig. 3). Given the large development data set (Moeser et al., 2015b) and the overall good performance of the parameterizations for the validation data set, it is reassuring that our models, perform sufficiently well in varying climate regions. This lends validity to the models for a range of coarse-scale model applications such as in climate, hydrologic (watershed and snow), and meteorological models.

     Despite the overall good performance of the models, we observed differences between the two validation data sets. The data

355   set collected in France shows improved error statistics for snow interception I_{HS} (e.g. for Eq. (3): NRMSE= 4 %, MAE= 0.28 cm, r= 1 and NRMSE$_{quant}$= 3 %) as compared to the data set collected in the U.S. (e.g. for Eq. (3): NRMSE= 14 %, MAE= 1.5 cm, r= 0.95 and NRMSE$_{quant}$= 12 %). In France, intercepted snow storm depth was measured as the difference of new snow depth in wooden boxes below trees and open area new snow storm depth. This was done in relatively short time intervals after a snow storm. In the U.S., intercepted snow was inferred from absolute snow depth differences before and after a snow storm

360   event within forests and in an open area. Derived snow interception was often integrated over several storm events due to longer periods between the measurement campaigns. Thus, these measurements were influenced by processes such as snow settling, wind redistribution, sublimation, unloading and melt. Our interception models do not account for such effects. We assume that these processes will be addressed separately, as in all prior interception models (Roesch et al., 2001). Our approach also does not define a maximum interception capacity, i.e. the maximum possible load on forest canopy (e.g. Schmidt and Gluns, 1991;

365   Hedstrom and Pomeroy, 1998; Roesch et al., 2001; Essery, 2013; Moeser et al., 2015a). ASifferences in model performances could also be attributed to the more accurate forest structure metrics for the French data set because of a higher resolution LiDAR DSM (higher point density of 24 /m^2 returns and 17 /m^2 last returns) compared to the LiDAR flyover from the U.S. (on average 7 returns/m^2 and 5 last returns/m^2). Despite some uncertainties in the validation data set from the U.S. it allowed for validation in a different snow climate than the French Alps and also covered a large spread in storm snowfall amounts (Fig.

370   4).

     To understand if the models would also work in other forest types or in disturbed forests, e.g. due to logging, fires or insect infestations, more snow interception measurements in deciduous and mixed as well as disturbed forests are required. Very recently Huerta et al. (2019) showed that previously published snow interception models developed for coniferous forests from Hedstrom and Pomeroy (1998); Lundberg et al. (2004); Moeser et al. (2016) required recalibration to match observed

375   point snow interception observations in a deciduous *Nothofagus* stand of the Southern Andes. We also investigated the model

performance for two measurement campaigns in a deciduous aspen (*Populous tremuloides*) forest in our U.S. field site. The measurement setup (20-m transects) was identical to the ones in the coniferous forest at this location (see Section 2.2). Though overall the models compared well with the measurements, the model performance was not as good as for the coniferous forest. Since the LiDAR DSM was acquired in the summer, i.e. with leaves on the trees, the models naturally overestimated I_{HS} and

380 $\sigma_{I_{HS}}$. For instance, using the more complex model for I_{HS} (Eq. (2)) we obtained a mean bias of -5.6 cm, respectively when using the more compact model for I_{HS} (Eq. (3)) we obtained a mean bias of -8.2 cm. For $\sigma_{I_{HS}}$, the performance was overall slightly better with a mean bias of -3.2 cm (Eq. (4)). While this shows that the performance is clearly lower in such sites, we assume that the performance would be improved when the LiDAR is acquired in leaf-off conditions.

The LiDAR derived DSM sky view factors do not account for small spaces between leaves or branches which are well

385 accounted for when sky view factors are derived from HP or LAI. In principle, sky view factors that are computed on DSM's represent, depending on the return signal used to create the DSM, a coarser view on the underlying forest canopy. While this increases fine scale error, we feel that the ability to calculate canopy structure metrics in the Cartesian DSM space far outweighs fine scale resolution losses.

Our choice for the functional form of P_{HS} differs from previous parameterizations for interception solely using the sigmoid

390 growth $\sim 1/(1 + exp(-k(P - P_0)))$ (e.g. Satterlund and Haupt, 1967; Schmidt and Gluns, 1991; Moeser et al., 2015b) or an exponential form $\sim (1 - exp(-k(P - P_0)))$ (e.g. Aston, 1993; Hedstrom and Pomeroy, 1998) with increasing precipitation and P_0 as the accumulated storm snow depth at the time of maximum interception efficiency. While the functional form of Satterlund and Haupt (1967) worked better for Moeser et al. (2015b), a drawback of this relationship is that interception does not become exactly zero for a zero snowfall amount. To account for this, the model becomes complicated when applied to

395 discrete model time steps (Moeser et al., 2016). For this reason, Mahat and Tarboton (2014) selected the relationship proposed by Hedstrom and Pomeroy (1998) for their parameterization of snow interception. However, the Hedstrom and Pomeroy (1998) model does not account for snow bridging or branch bending, thus modeling interception efficiency as decreasing through time. We also compared site means and standard deviations as a function of forest metrics and found that the use of storm means can introduce precipitation dependencies which might originate from an insufficient number of sites showing similar forest

400 canopy structure parameter values for a given precipitation (cf. black line compared to colored dots in Fig. (5)). Based on the functional dependencies revealed by analyzing our data as a function of P_{HS} and forest structure metrics, a simple power law was able to describe the P_{HS} dependency of snow interception (cf. Eq. (3)). The equation displayed that with increasing P_{HS}, I_{HS} increases. This is less pronounced with smaller σ_z or larger F_{sky} values (Fig. (5)). Despite an ongoing debate regarding the proper representation of interception, we believe that the interception models presented here can be applied in various model

405 applications for larger spatial scales.

6 Conclusion and Outlook

The statistical models for spatial mean and standard deviation of snow interception presented here are a first step towards a more robust consideration of snow interception for various coarse-scale model applications. They were built upon a very large

dataset and validated by two other datasets from different geographic regions and snow climates, and performed well for all

410   three sites and under differing weather conditions. For spatial mean interception all NRMSE's were ≤10 % and for the standard deviation of interception all NRMSE's were ≤13 %.

In all observed snow interception datasets, as much as 68 % and on average 43 % of the cumulative snowfall was retained by coniferous forests (interception efficiency of site means) and as much as 14 % and on average 11 % of the cumulative snowfall was retained by deciduous forests. Thus, these values compare well to previously observed snow interception in coniferous

415   trees reaching up to 60 % of cumulative snowfall and to 24 % of total annual snowfall in a deciduous forest in the Southern Andes.

The models integrate forest parameters that can be derived from fine-scale DSM's which can be pre-generated and stored for large regions. One of the presented interception models only relies on the standard deviation of the fine-scale DSM, which is a very efficient way to integrate snow interception in coarse-scale models such as land surface models. This could greatly

420   improve current forest albedo estimates and the subsequent surface energy balance for various model applications such as hydrological, weather and climate predictions.

However, the presented parameterizations were developed and validated for spatial means and standard deviations over horizontal length scales of a few tens of meters. We can only hypothesize that the parameterizations are also valid at coarser length scales due to the use of non-local forest structure parameters provided that a DSM of high enough resolution is available

425   to represent subgrid variability of forest structure in the coarse-scale model grid cell. However, there was and probably is, to-date, no validation data available at large spatial scales. The investigated length scale matches current satellite resolutions (e.g. Sentinel and Landsat) which opens further cross-validation and deployment opportunities with satellite-derived parameters such as surface albedos and fractional-snow covered area. With parameterizations for both, the mean and standard deviation of snow interception by forest canopy, the distribution of intercepted snow depth in forests can now be derived whenever a

430   sufficiently high-resolution DSM is available.

Competing interests.   The authors declare that they have no conflict of interest.

Acknowledgements.   We thank E. Thibert and É. Mermin, who performed GPS and tree measurements of the site setup at Col De Porte, and J.A. Lutz, S. Jones, J. Carlisle and D.G. Tarboton for their support and the possibility to work at TWDEF. N. Helbig was partly funded by the Federal Office of the Environment FOEN. M. Teich was partly funded by the Swiss National Science Foundation (P2EZP2_155606,

435   P300P2_171236), the Utah Agricultural Experiment Station (UAES), and the USU Department of Wildland Resources. The Labex SNOUF project has been supported by a grant from Labex OSUG2020-ANR10 LABX56. The TWDEF LiDAR data processing was supported by NSF EPSCoR cooperative agreement IIA 1208732 awarded to Utah State University, as part of the State of Utah Research Infrastructure Improvement Award. Any opinions, findings, and conclusions or recommendations expressed are those of the author(s) and do not necessarily reflect the views of the National Science Foundation.

References

Andreadis, K. M., Storck, P., and Lettenmaier, D. P.: Modeling snow accumulation and ablation processes in forested environments, Water Resour. Res., 45, https://doi.org/10.1029/2008WR007042, 2009.

Aston, A. R.: Rainfall interception by eight small trees, J. Hydrol., 42, 383–396, 1993.

Bartlett, P. A. and Verseghy, D. L.: Modified treatment of intercepted snow improves the simulated forest albedo in the Canadian Land Surface Scheme, Hydrol. Process., 29, 3208–3226, https://doi.org/10.1002/hyp.10431, http://dx.doi.org/10.1002/hyp.10431, 2015.

Bründl, M., Bartelt, P., Schneebeli, M., and Flühler, H.: Measuring branch deflection of spruce branches caused by intercepted snow load, Hydrol. Process., 13, 2357–2369, 1999.

Dirmeyer, P. A., Gao, X., Zhao, M., Guo, Z., Oki, T., and Hanasaki, N.: GSWP-2: Multimodel analysis and implications for our perception of the land surface, B. Am. Meteorol. Soc., 87, 1381–1398, 2006.

Essery, R.: Large-scale simulations of snow albedo masking by forests, Geophys. Res. Lett., 40, 5521–5525, https://doi.org/10.1002/grl.51008, 2013.

Essery, R., Rutter, N., Pomeroy, J., Baxter, R., Stähli, M., Gustafsson, D., Barr, A., Bartlett, P., and Elder, K.: SNOWMIP2: An evaluation of forest snow process simulations, Bull. Am. Meteorol. Soc., 90, 1120–1136, 2009.

Essery, R. L., Pomeroy, J. W., Parviainen, J., and Storck, P.: Sublimation of snow from coniferous forests in a climate model, J. Climate, 16, 1855–1864, 2003.

Essery, R. L., Bunting, P., Hardy, J., Link, T., Marks, D., Melloh, R., Pomeroy, J., Rowlands, A., and Rutter, N.: Scaling and parametrization of clear-sky solar radiation over complex topography, J. Hydrometeorol., 9, 228–241, 2008.

Hall, A.: The role of surface albedo feedback in climate, J. Clim., 17, 1550–1568, 2004.

Hedstrom, N. R. and Pomeroy, J. W.: Measurements and modelling of snow interception in the boreal forest, Hydrol. Process., 12, 1611–1625, 1998.

Helbig, N. and Löwe, H.: Parameterization of the spatially averaged sky view factor in complex topography, J. Geophys. Res., 119, 4616–4625, https://doi.org/10.1002/2013JD020892, 2014.

Helbig, N., Löwe, H., and Lehning, M.: Radiosity approach for the surface radiation balance in complex terrain, J. Atmos. Sci., 66, 2900–2912, https://doi.org/10.1175/2009JAS2940.1, 2009.

Hellström, R. A.: Forest cover algorithms for estimating meteorological forcing in a numerical snow model, Hydrol. Process., 14, 3239–3256, 2000.

Huerta, M. L., Molotch, N. P., and McPhee, J.: Snowfall interception in a deciduous Nothofagus forest and implications for spatial snowpack distribution, Hydrol. Process., 1-17, https://doi.org/10.1002/hyp.13439, 2019.

Knowles, N., Dettinger, M. D., and Cayan, D. R.: Trends in snowfall versus rainfall in the western United States, J. Climate, 19, 4545—-4559, 2006.

Krinner, G., Derksen, C., Essery, R., Flanner, M., Hagemann, S., Clark, M., Hall, A., Rott, H., Brutel-Vuilmet, C., Kim, H., et al.: ESM-SnowMIP: assessing snow models and quantifying snow-related climate feedbacks, Geosc. Model Dev., 11, 5027–5049, 2018.

Lejeune, Y., Dumont, M., Panel, J.-M., Lafaysse, M., Lapalus, P., Le Gac, E., Lesaffre, B., and Morin, S.: 57 years (1960–2017) of snow and meteorological observations from a mid-altitude mountain site (Col de Porte, France, 1325 m of altitude), Earth Syst. Sci. Data, 11, 71–88, https://doi.org/10.5194/essd-11-71-2019, https://www.earth-syst-sci-data.net/11/71/2019/, 2019.

Lundberg, A., Nakai, Y., Thunehed, H., and Halldin, S.: Snow accumulation in forests from ground and remote-sensing data, Hydrol. Process., 18, 1941–1955, https://doi.org/10.1002/hyp.1459, 2004.

Mahat, V. and Tarboton, D. G.: Canopy radiation transmission for an energy balance snowmelt model, Water Resour. Res., 48, 1–16, https://doi.org/10.1029/2011WR010438, 2012.

480   Mahat, V. and Tarboton, D. G.: Representation of canopy snow interception, unloading and melt in a parsimonious snowmelt model, Hydrol. Process., 28, 6320–6336, https://doi.org/10.1002/hyp.10116, 2014.

Moeser, D., Roubinek, J., Schleppi, P., Morsdorf, F., and Jonas, T.: Canopy closure, LAI and radiation transfer from airborne LiDAR synthetic images, Agric. For. Meteorol., 197, 158–168, 2014.

Moeser, D., Morsdorf, F., and Jonas, T.: Novel forest structure metrics from airborne LiDAR data for improved snow interception estimation, 485   Agric. For. Meteorol., 208, 40–49, 2015a.

Moeser, D., Staehli, M., and Jonas, T.: Improved snow interception modeling using canopy parameters derived from airborne LiDAR data, Water Resour. Res., 51, 5041–5059, https://doi.org/10.1002/2014WR016724, 2015b.

Moeser, D., Mazotti, G., Helbig, N., and Jonas, T.: Representing spatial variability of forest snow: Implementation of a new interception model, Water Resour. Res., 52, 5041–5059, https://doi.org/10.1002/2015WR017961, 2016.

490   Morin, S., Lejeune, Y., Lesaffre, B., Panel, J. M., Poncet, D., David, P., and Sudul, M.: An 18-yr long (1993-2011) snow and meteorological dataset from a mid-altitude mountain site (Col de Porte, France, 1325 m alt.) for driving and evaluating snowpack models, Earth Syst. Sci. Data, 4, 13–21, https://doi.org/10.5194/essd-4-13-2012, 2012.

Morsdorf, F., Kötz, B., Meier, E., Itten, K. I., and Allgöwer, B.: Estimation of LAI and fractional cover from small footprint airborne laser scanning data based on gap fraction, Remote Sens. Environ., 104, 50–61, 2006.

495   Pomeroy, J. W. and Schmidt, R. A.: The use of fractal geometry in modelling intercepted snow accumulation and sublimation, in: Proc. Eastern Snow Conference, vol. 50, pp. 1–10, 1993.

Pomeroy, J. W., Parviainen, J., Hedstrom, N., and Gray, D. M.: Coupled modelling of forest snow interception and sublimation, Hydrol. Process., 12, 2317–2337, 1998.

PRISM Climate Group: 30-Year Normals, Oregon State University, http://www.prism.oregonstate.edu/normals/ (created 07 November 2012); 500   accessed 28 June 2019, 2012.

Roesch, A. and Roeckner, E.: Assessment of snow cover and surface albedo in the ECHAM5 general circulation model, J. Clim., 19, 3828–3843, 2006.

Roesch, A., Wild, M., Gilgen, H., and Ohmura, A.: A new snow cover fraction parameterization for the ECHAM4 GCM, Clim. Dyn., 17, 933–946, 2001.

505   Roth, T. R. and Nolin, A. W.: Characterizing maritime snow canopy interception in forested mountains, Water Resour. Res., 55, https://doi.org/10.1029/2018WR024089, 2019.

Rousseeuw, P., Croux, C., Todorov, V., Ruckstuhl, A., Salibian-Barrera, M., Verbeke, T., Koller, M., and Maechler, M.: robustbase: Basic Robust Statistics, http://CRAN.R-project.org/package=robustbase, r package version 0.92-5, 2015.

Rutter, N., Essery, R., Pomeroy, J., Altimir, N., Andreadis, K., Baker, I., Barr, A., Bartlett, P., Boone, A., Deng, H., et al.: Evaluation of forest 510   snow processes models (SnowMIP2), Journal of Geophysical Research: Atmospheres, 114, 2009.

Satterlund, D. R. and Haupt, H. F.: Snow catch by conifer crowns, Water Resour. Res., 3, 1035–1039, https://doi.org/10.1029/WR003i004p01035, 1967.

Schmidt, R. A. and Gluns, D. R.: Snowfall interception on branches of three conifer species, Can. J. For. Res., 21, 1262–1269, 1991.

Sicart, J. E., Essery, R. L. H., Pomeroy, J. W., Hardy, J., Link, T., and Marks, D.: A sensitivity study of daytime net radiation during snowmelt

515   to forest canopy and atmospheric conditions, J. Hydrometeorol., 5, 774–784, 2004.

Siegel, R. and Howell, J. R.: Thermal Radiation Heat Transfer, Hemisphere Publishing Corp., 1978.

Storck, P. and Lettenmaier, D. P.: Measurement of snow interception and canopy effects on snow accumulation and m elt in a mountainous

maritime climate, Oregon, United States, Water Resour. Res., 38, https://doi.org/10.1029/2002WR001281, 2002.

Suzuki, K. and Nakai, Y.: Canopy snow influence on water and energy balances in a coniferous forest plantation in Northern Japan, J. Hydrol.,

520   352, 126–138, 2008.

Teich, M. and Tarboton, D. G.: TW Daniels Experimental Forest (TWDEF) Lidar, HydroShare,

https://doi.org/10.4211/hs.36f3314971a547bc8bc72dc60d6bd03c, 2016.

Teich, M., Giunta, A. D., Hagenmuller, P., Bebi, P., Schneebeli, M., and Jenkins, M. J.: Effects of bark beetle attacks on for-

est snowpack and avalanche formation – Implications for protection forest management, For. Ecol. Manage., 438, 186 – 203,

525   https://doi.org/10.1016/j.foreco.2019.01.052, 2019.

Varhola, A., Coops, N., Weiler, M., and Moore, R. D.: Forest canopy effects on snow accumulation and ablation: An integrative review of

empirical results, J. Hydrol., 392, 219–233, 2010.

Vincent, L., Lejeune, Y., M, L., Boone, A., Gac, E. L., Coulaud, C., Freche, G., and Sicart, J. E.: Interception of snowfall by the trees is the

main challenge for snowpack simulations under forests, in: Proceedings of the International Snow Science Workshop (ISSW), Innsbruck,

530   Austria, pp. 705–710, http://arc.lib.montana.edu/snow-science/objects/ISSW2018_O08.4.pdf, 2018.

Webster, C. and Jonas, T.: Influence of canopy shading and snow coverage on effective albedo in a snow-dominated evergreen needleleaf

forest, Remote Sens. Environ., 214, 48 – 58, 2018.
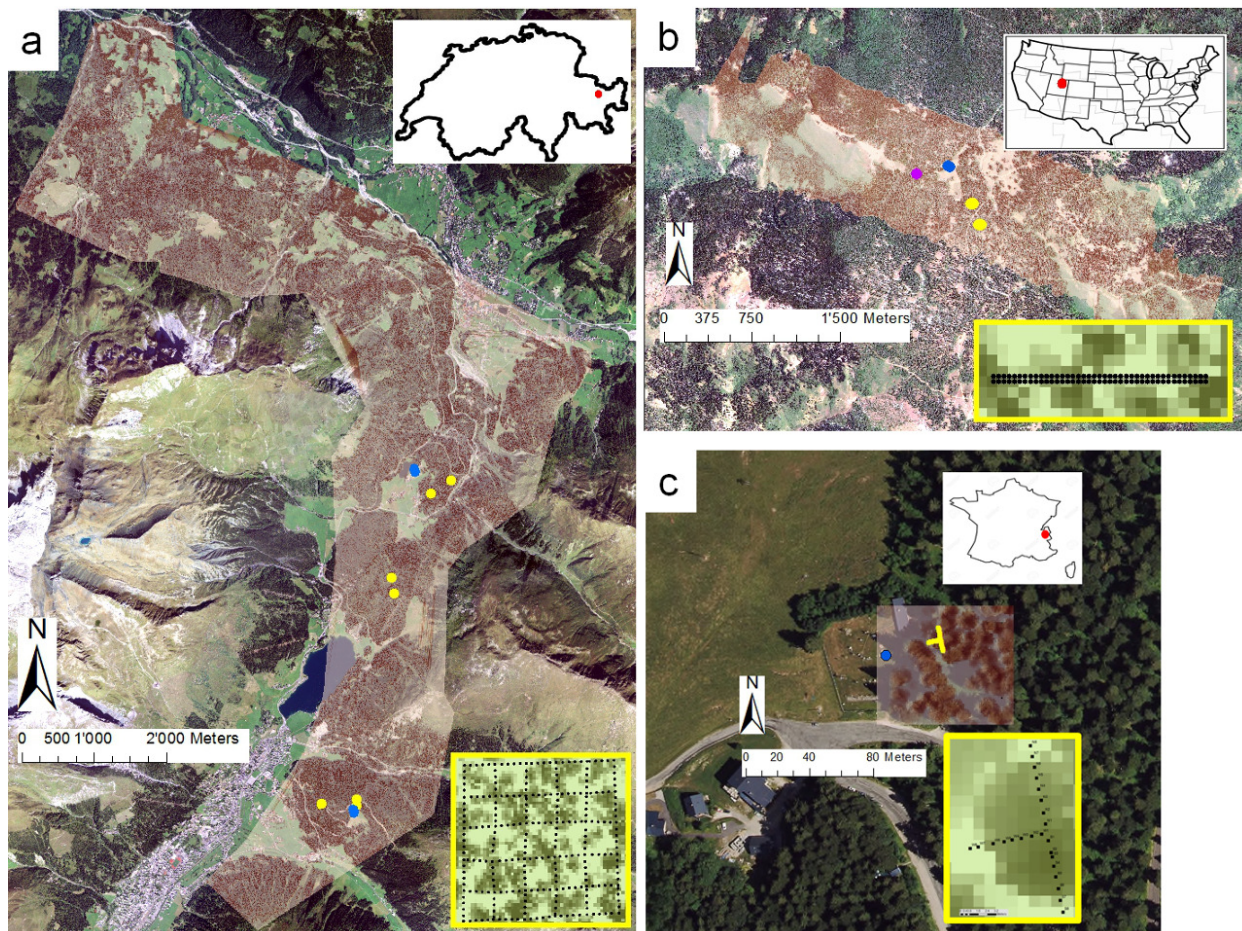
Figure 1. Extent of lidar derived tree DSM's with locations of open (blue points), forested field sites (yellow points) and SNOTEL site (purple point): (a) close to Davos in the Eastern Swiss Alps ($\sim$90 km^2), (b) in the Rocky Mountains of Northern Utah, U.S. ($\sim$13km^2), and (c) in the Southeastern French Alps at Col de Porte ($\sim$0.01 km^2). The yellow framed inlets show the respective snow depth measurement setup at the forested field sites. Underlying orthophotos for the French site were provided by IGN (France) and for the Swiss site by Swisstopo (JA100118). For the site in the U.S. © Google Earth imagery was used.
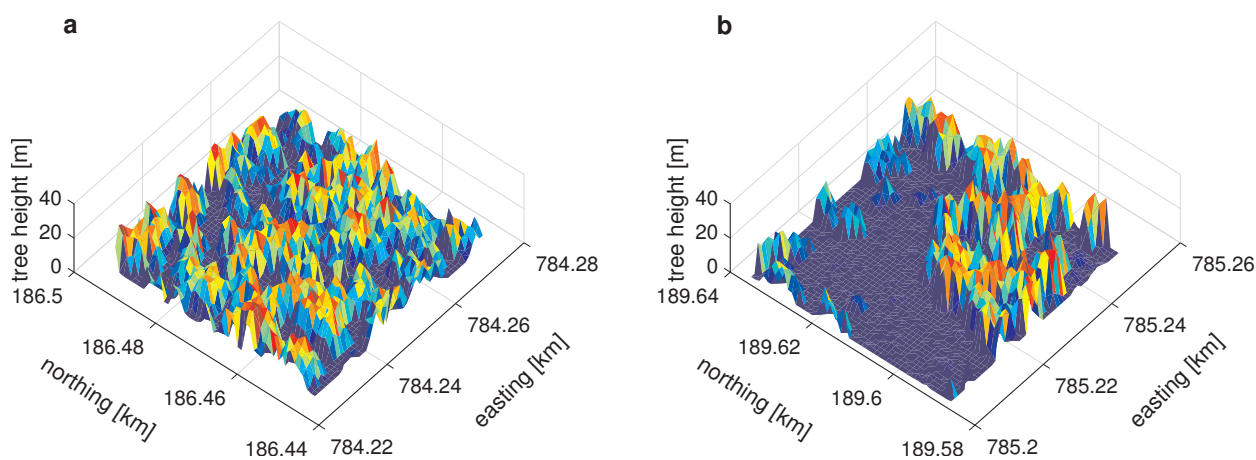
Figure 2. Tree DSM's for two 50 x 50 m^2 field sites in the Eastern Swiss Alps with (a) high canopy coverage and (b) low canopy coverage (for detailed site descriptions see Moeser et al., 2014).
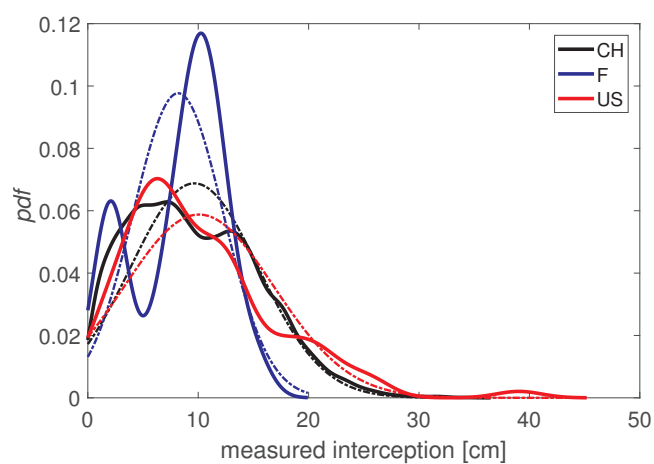
Figure 3. Probability density functions (*pdf*'s) of all individual snow depth interception measurements used for the development (Swiss (CH) data set) and for the validation of the parameterizations (French (F) and US data sets) The dashed lines indicate a theoretical normal *pdf* for the corresponding data set.
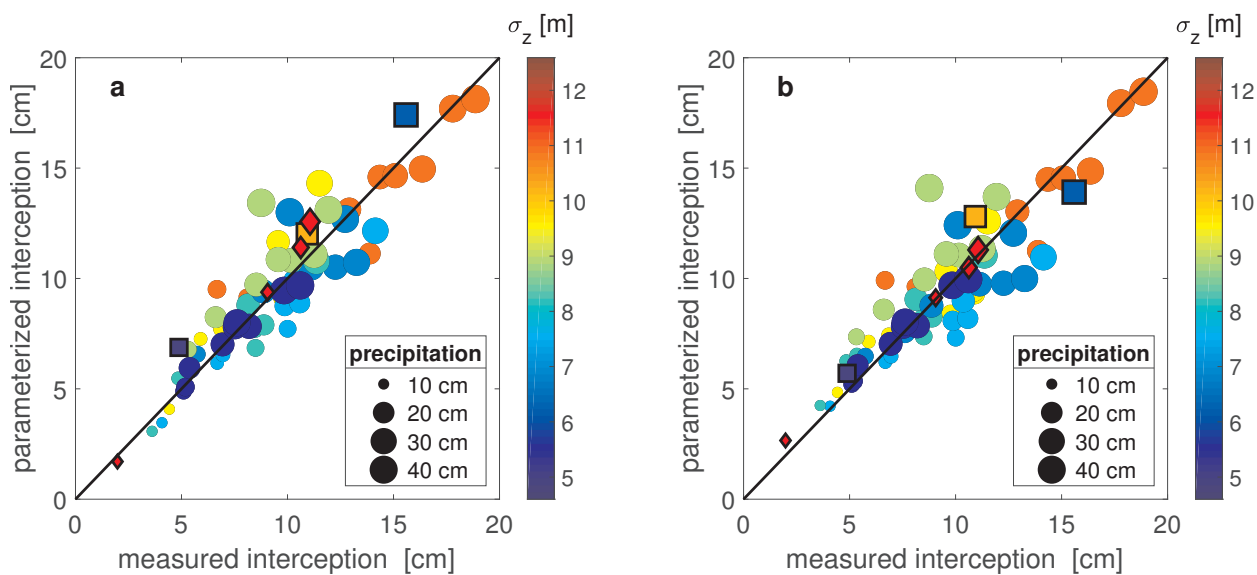
Figure 4. Measured and parameterized site means of intercepted snow depth, i.e. spatially averaged over each site and for each storm date. Parameterized using a) Eq. (2) and b) Eq. (3) as a function of site means of standard deviation of the lidar DSM σ_z (in color) as well as open area snow storm precipitation (size of symbols). Circles represent the development data set from Switzerland, symbols with a black border represent the validation data sets with squares for that from the U.S. and diamonds for that from France.
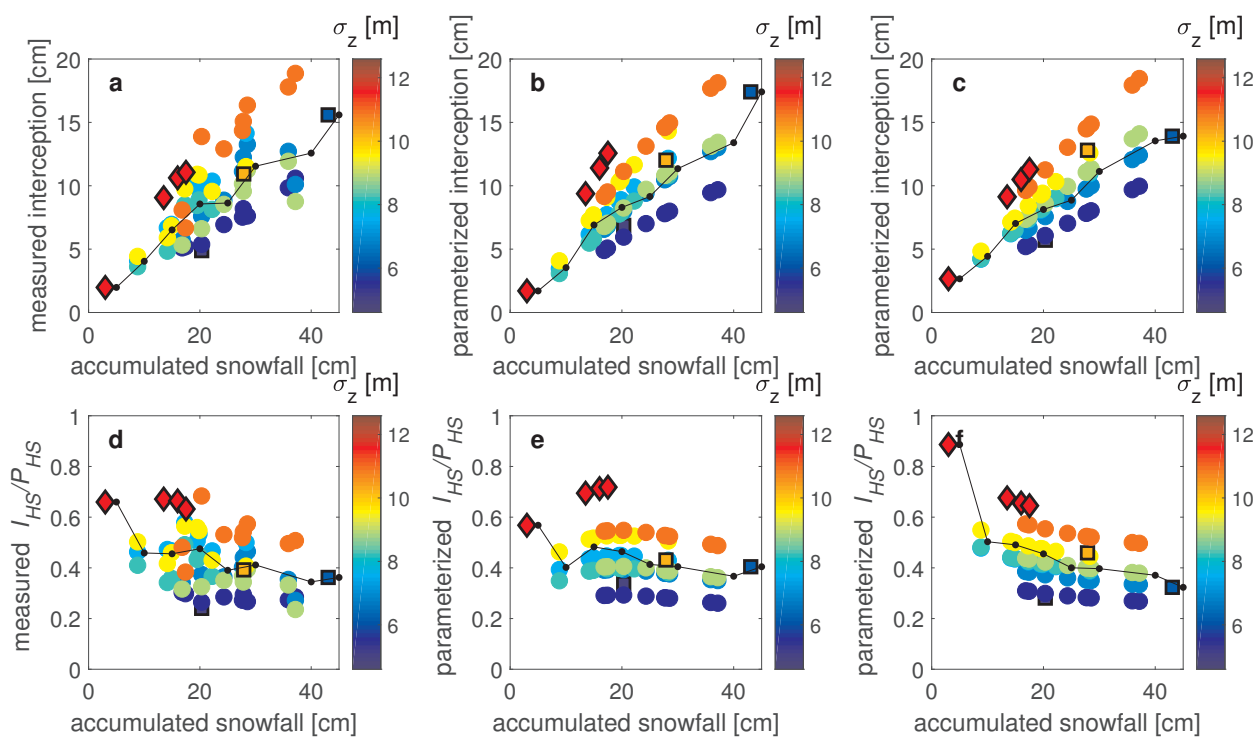
Figure 5. Snow depth interception I_{HS} (a,b,c) and interception efficiency I_{HS}/P_{HS} (d,e,f) as a function of accumulated open area snow storm precipitation P_{HS} and standard deviation of the lidar DSM σ_z (in color). The y-axis of the first column shows measured data, the second column shows model output with Eq. (2) and the third model output with Eq. (3). Site means for each storm event are depicted with colored circles for the development data set from Switzerland and symbols with a black border depict the validation data sets, with squares for that from the U.S. and diamonds for that from France. Storm means (in P_{HS} bins) are shown in black.
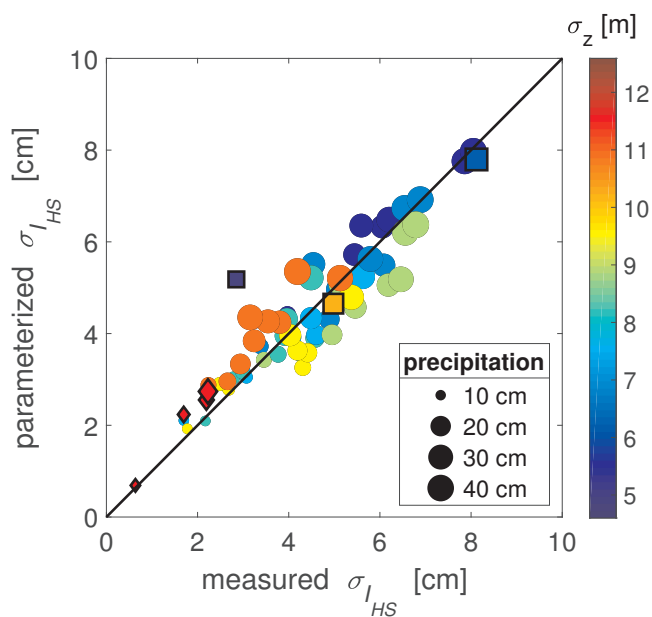
Figure 6. Measured and parameterized standard deviation of snow depth interception $\sigma_{I_{HS}}$ at each site and for each storm date. Parameterized using Eq. (4) as a function of site means of standard deviation of the lidar DSM σ_z (in color) as well as open area snow storm precipitation (size of symbols). Circles represent the development data set from Switzerland, symbols with a black border represent the validation data sets with squares for that from the U.S. and diamonds for that from France.

Table 1. Performance measures between measurement and parameterization of spatial-mean snow depth interception I_{HS} with (a) Eq. (2), (b) with Eq. (3)), and (c) standard deviation of snow depth interception $\sigma_{I_{HS}}$ with Eq. (4). Statistics are shown for the development data set from the Eastern Swiss Alps (CH) and for the combined validation data set (U.S.&F).

	NRMSE	RMSE	MPE	MAE	r	K-S	NRMSE$_{\text{quant}}$
a) I_{HS} (Eq. (2))							
CH	9.0	1.37	-2.0	1.02	0.92	$8.6\,10^{-2}$	2.2
U.S.&F	9.4	1.28	-10.43	1.11	0.99	$4.3\,10^{-1}$	9.9
b) I_{HS} (Eq. (3))							
CH	10.2	1.55	-2.87	1.15	0.89	$1.0\,10^{-1}$	4.9
U.S.&F	7.6	1.04	-8.45	0.78	0.97	$2.9\,10^{-1}$	6.2
c) $\sigma_{I_{HS}}$ (Eq. (4))							
CH	8.9	0.57	-2.04	0.45	0.92	$8.6\,10^{-2}$	3.9
U.S.&F	12.7	0.95	-21.52	0.64	0.94	$4.3\,10^{-1}$	10.4